Numerical Analysis of Transcranial Magnetic Stimulation Application in Patients With Orofacial Pain

David Vrba, *Member, IEEE*, Lukas Malena, Jakub Albrecht, Jitka Fricova, Martin Anders, Richard Rokyta, Dario Rodrigues, and Jan Vrba, *Member, IEEE*

***Abstract*— In this paper, we monitored the accuracy of non-navigated application of repetitive Transcranial Magnetic Stimulation (rTMS) in 10 patients suffering from orofacial pain by using functional magnetic resonance (fMRI), computer modeling and numerical simulation. Through a unique process, each fMRI scan was used to define a Region of Interest (ROI) where the source of the orofacial pain was located, which was to be stimulated using rTMS. For each patient, MRI scans with a spatial resolution of 0.7 mm were converted into an anatomically accurate head model. The head model including the ROI was then co-registered with a model of the stimulation coil in an electromagnetic field numerical simulator. The accuracy of rTMS application was evaluated based on the calculations of electric field intensity distribution in the ROI. The research has yielded unique insight into ROIs (with average volume 904 mm^3) in patients with orofacial pain and has also extended further possibilities of human head MRI image semi-automatic segmentation. According to the calculations performed, the average ROI volume that was stimulated by an electric field with an intensity of over 80 V/m was only 4.4%, with the maximum ROI volume being 20.5%. Furthermore, a numerical study of the impact of coil rotation and translation was performed. It demonstrated a) the optimal placement of the stimulation coil can significantly increase the volume of the stimulated ROI up to 60% and b) patients with orofacial pain would need precise coil positioning with a navigation error lower than 10 mm. Due to an acceptable proccessing time of up to 6 hours, described numerical simulation opens up new options for precise rTMS treatment planning. This planning platform together with patient-specific navigated rTMS, could lead to significant increase of treatment outcomes in patients suffering from orofacial pain.**

***Index Terms*— Orofacial pain, transcranial magnetic stimulation, numerical model.**

I. Introduction

REPETITIVE Transcranial Magnetic Stimulation (rTMS) is becoming a promising therapeutic approach in the fields of psychiatry [1] and physical rehabilitation [2]. Using an external coil adjacent to the head, rTMS delivers strong magnetic pulses that induce electrical currents in brain [3]. The induced electrical field (E-filed) causes neuronal membrane potential changes that reduce neuronal activity. This therapy is relatively painless and non-invasive [4].

Orofacial pain includes dental pain, musculoskeletal disorders, neuropathy or neoplasia. Pain from these sources is usually treated via surgery or pharmaceutical drugs. There are some patients, however, who suffer from an uncommon type of chronic orofacial pain who do not respond to the aforementioned treatments. In these cases, the ability of rTMS to suppressneural activity in brain regions responsible for sensing orofacial pain makes rTMS a potentially viable treatment [5], [6].

Wherever localized, the pain is triggered by overreacting sensory neuron receptors. Neurons in the sensory cortex process the signal of orofacial pain transmitted by sensory neurons that can be also externally activated by mechanical stimulation. Therefore, a small area in the sensory cortex where activated neurons are displayed using fMRI intersects the area which is somototopicaly related with orofacial pain collectively forming the source of orofacial pain: This source is marked and thus determined as the region of interest (ROI) to be stimulated by rTMS.

There are many studies exploring optimal coil geometries and the relationship between the ability to focus the elec-

Manuscript received June 25, 2021; revised December 11, 2021 and February 4, 2022; accepted March 1, 2022. Date of publication March 3, 2022; date of current version March 17, 2022. This work was supported in part by the Czech Science Foundation under Grant 21-00579S, in part by the Czech Technical University in Prague (CTU) under Grant SGS20/203/OHK4/3T/17, and in part by the Ministry of Health of the Czech Republic under Grant MH CZ—DRO VFN64165. *(Corresponding author: David Vrba.)*

This work involved human subjects or animals in its research. Approval of all ethical and experimental procedures and protocols was granted by the Ethical Committee of the Third Faculty of Medicine, Charles University, Prague, Czech Republic, under Protocol No. 122240.

David Vrba, Lukas Malena, and Jan Vrba are with the Department of Biomedical Technology, Faculty of Biomedical Engineering, Czech Technical University in Prague, 166 36 Prague, Czech Republic (e-mail: david.vrba@fbmi.cvut.cz; lukas.malena@fbmi.cvut.cz; jan.vrba@fbmi.cvut.cz).

Jakub Albrecht is with the Department of Psychiatry, Krajska zdravotni, as Most Hospital, 434 01 Most, Czech Republic (e-mail: jakub.albrecht@kzcr.eu).

Jitka Fricova is with the Pain Management Center, Department of Anesthesiology and Intensive Care, First Faculty of Medicine, Charles University in Prague and General University Hospital in Prague, 116 36 Prague, Czech Republic (e-mail: jitka.fricova@vfn.cz).

Martin Anders is with the Department of Psychiatry, First Faculty of Medicine, Charles University and General University Hospital in Prague, 116 36 Prague, Czech Republic (e-mail: martin.anders@vfn.cz).

Richard Rokyta is with the Department of Physiology, Third Faculty of Medicine, Charles University, 180 00 Prague, Czech Republic (e-mail: richard.rokyta@lf3.cuni.cz).

Dario Rodrigues is with the University of Maryland School of Medicine, Department of Radiation Oncology, Baltimore, MD 21201 USA (e-mail: drodrigues@som.umaryland.edu).

This article has supplementary downloadable material available at https://doi.org/10.1109/TNSRE.2022.3156703, provided by the authors.

Digital Object Identifier 10.1109/TNSRE.2022.3156703

tric field and its penetration depth [7]–[10]. The most used applicator geometry is a figure-eight shaped coil that generates a high-intensity electrical field focused to small volume. Once the coil is selected, an optimal position must be determined to target the brain area expected to be the source of the issue.

Despite the available neuronavigation tools anthropometric method of determining the location of the area to be stimulated is still beeing used. This method takes measurements between anatomically significant points and translates them using table values to find the stimulation center. The parasagittal coplanar transposition method [11] does not take into account individual brain anatomy and is based purely on statistics. Following the current recommendations, medical doctors try to keep the coil at an angle of 45° to the mediosagittal plane. This orientation ensures that the main component of electric field is perpendicular to the gyrus wall, which has the ability to increase electric field intensity and trigger changes in neuron membranes.

Suboptimal coil position leads to electric field intensity changes that could reduce the neuromodulation effect in the ROI and/or involve stimulation of other brain regions. However, the coil rotation considered in [12] is just one of many degrees of freedom of the mutual position of the stimulation coil and the patient's head.

From a technical standpoint, the coil position and E-field distribution are the key parameters to monitor when performing rTMS. From a medical standpoint, head and brain anatomy has a significant impact on the distribution of the electric field. In our patients, physiological as well as pathological anatomy was considered. Direct monitoring of the electromagnetic field in the stimulated subject is not possible. The information about the distribution of the electric field in a patient's head can be calculated with numerical simulations using a virtual model [13].

In [14], the homogeneous spherical head model was used for the numerical modeling of rTMS electric field induced in a human head. This model simplifies the material and geometric characteristics of a human head. A logical trend in rTMS modeling are so-called anatomically accurate models [15]. Commercially available anatomical models based on MRI image segmentation are especially popular today [16]–[18]. In comparison to the simplified ones, they take into account the geometry of the individual cerebral gyri, thus enabling a more accurate calculation of the resulting induced electric field.

The results of previous studies indicate that the following solutions can be used to calculate electrical field distribution: low-frequency solvers using quasi static approximation [19], modified finite-difference time-domain method [20], finite element method [21]–[23], surface integral equation [24]. Analytical methods have also been used to simulate E-fields, but only for simplified brain model geometries [14].

The main goals of this paper are two-fold: 1) to calculate the electric field intensity in ROI in patients undergoing rTMS application for possible relief of orofacial pain; and 2) to identify which of the examined coil position changes are the key factors affecting the induced E-field intensity during rTMS application. In the procedure, fMRI scans with a resolution of 0.7 mm will be used to create anatomically accurate head models. Each model includes a ROI where the source of the orofacial pain is located and must be stimulated using rTMS. For each patient, the stimulation coil and anatomical head models will be co-registered in the electromagnetic field simulator for a precise calculation of the induced E-field. The calculated electric field distribution in the ROI aims to reveal individual therapeutic effects achievable with standard coil positioning. Next, the study of the impact of the rotation and translation of the coil will be performed to identify key factors responsible for the changes in the intensity of the E-field.

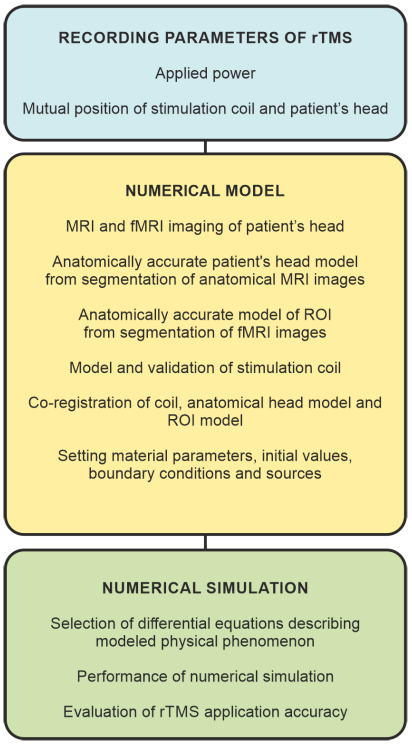

Fig. 1. Numerical workflow to evaluate retrospectively the rTMS treatment accuracy.

II. Methods

The following sections describe the steps required for modeling of rTMS treatments to perform an in silico retrospective assessment of the clinical parameters used for treatment (Fig. 1).

The study was reviewed and approved by the ethical committee of the Third Faculty of Medicine, Charles University, Prague, Czech Republic, the protocol No. 122240. All subjects signed the informed consent accordingly.

A. Recording rTMS Therapy Parameters

A total of 10 patients was treated with rTMS for treatment of orofacial pain. The clinical data collection for these patients is described below.

1) Recording the Stimulation Coil Position Relative to the Human Head: The stimulation coil used in the rTMS treatments was the Magstim 70 mm Double Air Film Coil (The Magstim Company Ltd., Spring Gardens, UK). Before each treatment, the target area for stimulation in the sensory cortex was determined using parasagittal coplanar transposition [11].

The final position of the stimulation coil was plotted on a polyester cap to exclude the patient movements. Then, a 3D scan was performed to record coil nad head positions using the KINECT Fusion Explorer software [25] together with the KINECT for Xbox One sensor by Microsoft, which employs camera and infrared dot matrix triangulation. The resulting 3D head model was imported into the electromagnetic field simulator Sim4Life v3.4 (ZMT Zürich MedTech AG, Switzerland), which already contained the coil model. Supplementary Table I lists the parameters used to set up KINECT Fusion Explorer.

The method's accuracy was verified by measuring the distance between the marked points on the patient's head and on the digital representation, i.e. on the 3D scans, in order to determine the dimension variance.

2) Parameters of rTMS: For each patient, an individual trigger point value was recorded. The trigger point value was determined by gradually increasing stimulator output given by the amplitude of the electric current flowing through the stimulation coil winding. The trigger point was considered to be set when eight out of ten pulses elicited musculus abductor pollicis brevis motor response. By using the parasagittal coplanar transposition method the stimulation coil was placed above the sensory cortex. The stimulator was then set to the 50 Hz theta burst stimulation mode with current output at 90% of the motor threshold containing 660 pulses in six trains with the desired inhibition effect.

3) Verification of the Magnetic Field Generated by the Stimulation Coil: In order to validate numerical simulations, the stimulation coil parameters were tested in an air phantom box. First, the waveform and duration of the stimulation pulse were measured, followed by the measurement of magnetic flux density values in the vicinity of the actual stimulation coil. The magnetic field was verified in the average distance between the stimulation coil winding and the centre of gravity of the ROIs that were the focus of rTMS therapy. The measurements were performed on a plane at a distance of 34 mm from the centre of the stimulation coil winding (Z-axis). On the selected X-Y plane, an area ±30 mm along the Y-axis was measured in 10 mm steps, centred at the point of the highest magnetic field induction. To increase measurement sensitivity, a coil consisting of 10 planar layers was used as the magnetic field measurement sensor [26]. A system of 5 holders of different lengths was used to facilitate changes in position ±20 mm along the X-axis.

The measuring coil winding plane was perpendicular to the lines of the magnetic field generated by the stimulation coil. The measuring coil output was connected to the input of the Keysight DS0-X 4024A oscilloscope probe as shown in Fig. 2. The pulse settings used in the stimulator (Magstim Rapid2) were "Single Pulse" mode and maximum output. Finally, an equivalent model matching this experiment was created in Sim4Life. The experimental and simulated voltages induced in the measuring coil were then compared for validation of the numerical modeling approach.

B. Virtual Model

The virtual model of each patient includes an anatomically accurate head including the target (ROI) and the stimulation coil. All models are co-registered in the numerical simulator according to the 3D scan recorded during the rTMS session.

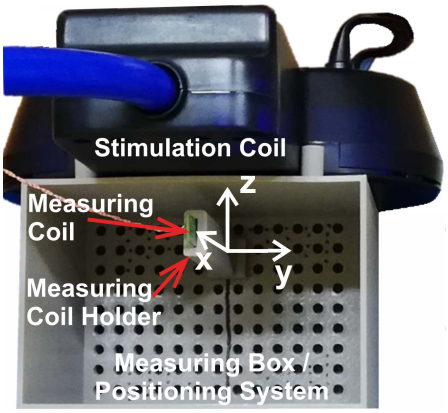

Fig. 2. Experimental setup for magnetic field measurements: air phantom box containing the measuring coil; and stimulation coil (blue).

1) Anatomically Accurate Head Model: The geometry of each anatomically accurate head model was obtained via segmentation of tissue structures from the patient MR images. These images were acquired using a 3T system Magnetom Prisma (Siemens, Germany) together with the 64-channel head and neck RF coil (Siemens, Germany). The MR sequence used was MPR 3D Connectom: TR 2400 ms, TE 2.34 ms, TI 1000 ms with a image matrix resolution $320 \times 320 \times 240$ pixels. For segmentation, we used the MARS (Morphologically and Anatomically accuRate Segmentation) [27] throughout the study. This software is based on a strict decision-making model that combines an intensive image model, anatomical prior atlas and morphological limitations using random Markov fields (MRF). This method enabled us to get higher-quality transitions between individual tissues, in contrast to current methods of statistical parametric mapping (SPM). The MARS segmentation tool is also significantly faster to segment the different structures. The code and the data are fully implemented in the SPM8 software [28].

The geometry of the patient's anatomically accurate head models was created using three steps. First, we used MARS for automatic segmentation of individual tissues: skin, skull, cerebrospinal fluid, grey matter, white matter and air-filled cavities. Second, we converted 2D segmented images into a 3D anatomically accurate computer model using the iSeg software (ZMT Zürich MedTech AG, Switzerland) [29]. The iSeg tool was used to perform manual inspections of the MR images to eliminate inhomogeneities and random errors generated by MARS. The resulting models were imported into the Sim4Life simulator. The third and last step - was fMRI processing. The region of the face where the patient reported the pain, was stimulated mechanically during fMRI using a custom-made tool based on von Frey filaments. Data from the fMRI was processed using a SPM program to find neural activations [28]. fMRI images containing highlighted neural activation voxels are converted to a 3D model using iSeg. The fMRI image matrix with the same size as the MR image matrix was then co-registered with the resulting anatomically accurate computer model in Sim4Life. Based on the somatotopic arrangement of the brain and the patient's

TABLE I
DIELECTRIC PROPERTIES OF TISSUES @ 3300HZ [31]

Material/tissue	Material parameters		
	σ (S/m)	ε_r(-)	μ_r(-)
Air	0.00	1	1
Skin	0.17	1135	1
Skull	0.32	1156	1
Cerebrospinal Fluid	1.77	109	1
Grey Matter	0.24	61500	1
White Matter	0.27	28170	1

diagnosis, the physician selected the appropriate intersection of neural activation and the grey matter model located in the sensory cortex considered the ROI. With the anatomical model completed, each tissue was assigned electrical conductivity (σ), relative permittivity (ε_r) and relative permeability (μ_r) properties (Table I) retrieved from [30], [31]. The relative permittivity and permeability of tissues are listed only with regard to fulfilling the criteria of using quasi static approximations discussed in Sec II-C.

2) Coil Model and Co-Registration: The virtual model of the stimulation coil was created based on measurements derived from Computed Tomography (CT) scans. In the numerical simulator, an harmonic electric current with a fixed amplitude and phase was defined for the whole length of the winding. The coil model was then co-registered with the patient's head in Sim4Life by gradually adjusting the positions of both models to match the 3D scan.

C. rTMS Computer Simulation

Numerical simulations of induced electric field intensity distribution in a patient's brain, were performed in the commercial electromagnetic field numerical simulator Sim4Life 3.4 [32]. The stimulation current frequency of 3300 Hz in the Magstim system [33], the dielectric and magnetic properties of biological tissues (listed in Table I) and the physical dimensions of the virtual model, satisfy the criteria for quasi static approximation with only ohmic losses [32]:

$$\omega^2 \varepsilon \mu d^2 \ll 1, \quad \omega\sigma\mu d^2 \ll 1, \ \omega\varepsilon/\sigma \ll 1, \tag{1}$$

where ω is the signal's angular frequency, ε, σ, μ are electric permittivity, electric conductivity and magnetic permeability of the tissue, respectively, and d is the largest dimension of the computational domain (the diagonal of a cube surrounding the computational domain). All criteria were met, even for the least favorable material constant and frequency combinations.

This approach determines the distribution of static vector magnetic potential in the whole computational domain merely by applying the Biot-Savart law [32] and assuming time-harmonic electric current with constant amplitude and phase on the whole stimulation coil winding. Intensity of the induced electric field is calculated in lossy dielectric environment – biological tissues – by solving the potential continuity equation. The numercal simulation was performed on a workstation with the following relevant technical specifications: Intel® Core(TM) i7-3820 @ 3.60 GHz, 48 GB RAM and 1 TB SSD.

Therefore, the numerical simulation in Sim4Life included: Electromagnetic Field – Low Frequency (EMLF), Magneto Quasi Static, Ohmic losses dominated.

1) Evaluation of the Results of Numerical Simulations: The numerical simulations results in the spatial distribution of the electric field intensity vector induced in the anatomically accurate head models of individual subjects' heads. For the purposes of evaluating the precise targeting of stimulating patients with orofacial pain, a ROI was introduced, to the region where activation occurs, as already introduced in II-B.1. The electromagnetic field simulator considers each tissue created by image segmentation to be homogenous body. Numerical simulation calculates the absolute maximum values of electric filed intensity vector achieved during one period of stimulation pulse. The stimulation targeting was then evaluated by calculating the volume and percentage of ROI where an intensity of electric field is over 80 V/m [34], [35]. To optimize the position and orientation of the coil, a copy of the stimulation coil was created in each patient's model and moved above the ROI's center of gravity.

2) Analysis of the Effect of Coil Rotation and Translation on the Accuracy of rTMS: Since the coil position relative to the ROI proved to be very significant, an analysis of the influence of coil rotation and coil translation was performed in one representative patient. The rotations and translations were performed according to the coordinate system shown in Fig. 3. For this analysis, we chose subject no. 3 with the ROI close to the average value while maintaining the original stimulation current amplitude. Fig. 3A shows the initial coil position that was set to be parallel to grey matter surface and perpendicular to the gyrus wall. The coil was then rotated with a 90° step around the Z-axis as seen in Fig. 3B. The coil was also rotated by ±15° from the initial position around the X-axis, as shown in Fig. 3C and translated along the X- and Y-axes by ±2 cm, as shown in Figs. 3D and E, respectively. The next step was to rotate the coil around the Z-axis by 90° to get the coil into a position parallel to the grey matter surface and the gyrus wall. These coil rotations and translations about and along the X- and Y-axes were repeated in the 90° position.

III. RESULTS

A. Magnetic Field Measurement Results

Time evolution of the measured voltage induced in the measuring coil, and time evolution of the induced magnetic flux density are plotted in Fig. 4. From the pulse length time of 303 μs, the stimulation pulse frequency of 3300 Hz was calculated. Since the measurement was, on average, 28 percent lower than the simulation data, see Fig. 5, the current flowing through the stimulation coil is probably lower than stated by the manufacturer. For this reason, the current flowing through the coil was correspondingly reduced to 3900A for the simulation, so that the simulation values matched the measurements. Table II lists the adjusted stimulation current values that match the measured values.

B. Three-Dimensional Scan Results

Fig. 6 shows an example result of the 3D scan of the stimulation coil position in relation to the patient's head. The most consistent 3D scan geometry was obtained with scan times under 20 seconds. Another approach that proved

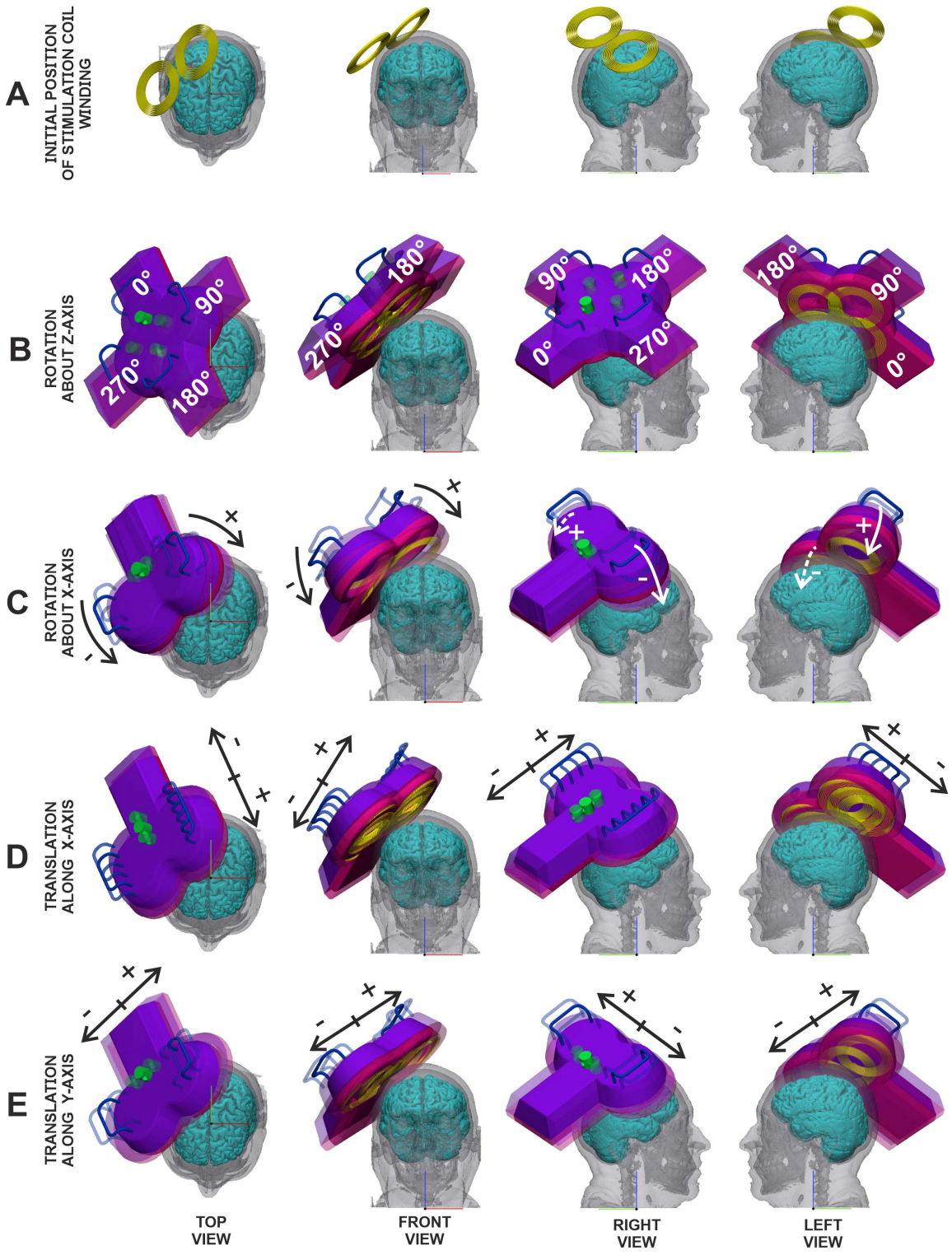

Fig. 3. (A) Initial position of the activation under the stimulation coil winding, (B) Rotation of the rTMS coil around the Z-axis, (C) Rotation of the stimulation coil around the X-axis in the initial position, (D) Translation along the X-axis and (E) Y-axis in the initial position. The model of coil winding consists of a 9 turn-spiral with inner and outer radius of 27 and 45 mm respectively.

beneficial was to move the KINECT sensor slightly in front of the patient face. When the KINECT sensor is moved a larger angle and the KINECT Fusion Explorer software need to build larger part of scan, the geometry is not smooth and precise. A 3D scan error analysis was performed and its results are summarized in Supplementary Table II.

C. MRI and fMRI Results

The result of statistical evaluation of fMRI images using the SPM software is a color map illustrating signal change in the area under examination. Fig. 7 shows the result of the statistical evaluation of fMRI images of subject no. 8, projected into a T1 scan for easier orientation. Neural activation for this subject is

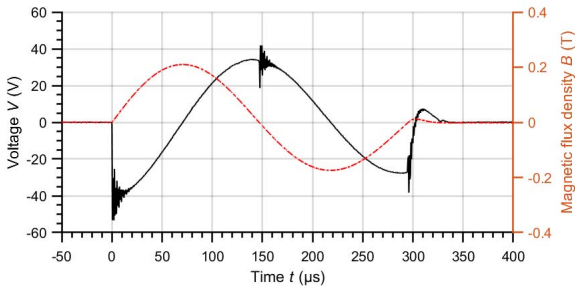

Fig. 4. Pulse wave at point 0;0, 34 mm from the AirFilm coil winding.

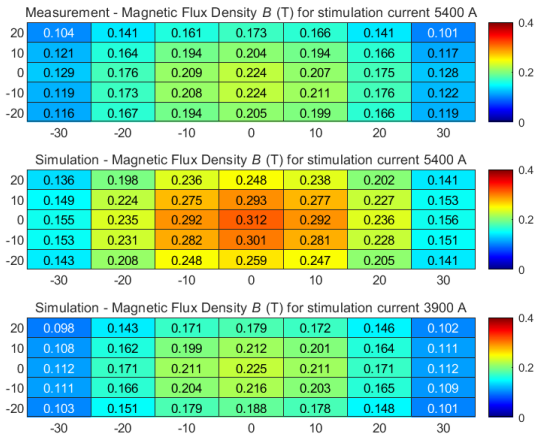

Fig. 5. Graphical comparison of magnetic induction distribution measured (top), simulated (middle) and simulated with reduced stimulation current (bottom) on a plane; the distance between the plane and the stimulation coil winding is 34 mm.

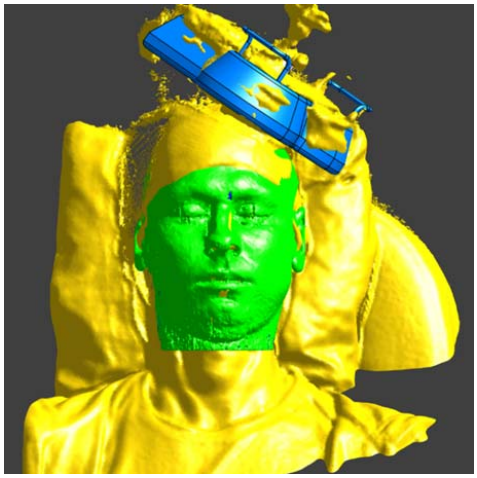

Fig. 6. Stimulation coil model (blue) and an anatomically accurate head model (green) co-registered with a 3D scan of the patient and the coil (yellow).

located in the sensory cortex of the right hemisphere. Of the multiple areas where signal change occurred, only the part intersected with sensory cortex was considered.

Fig. 8 shows the results of MRI image segmentation for subject no. 8. For the purposes of this study, five different biological tissues and one non-tissue material were differentiated: skin, skull, cerebrospinal fluid, grey matter, white matter

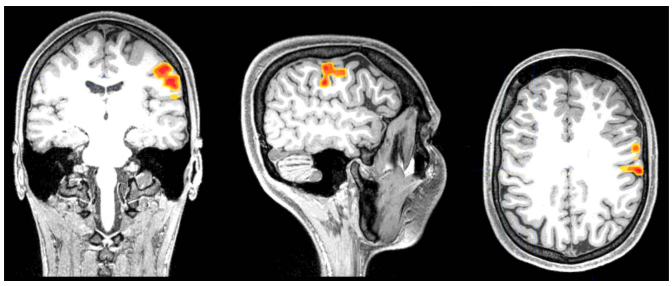

Fig. 7. Processed fMRI images for subject no. 8, co-registered with the T1 scan. Activation is visible in the sensory cortex of the right hemisphere.

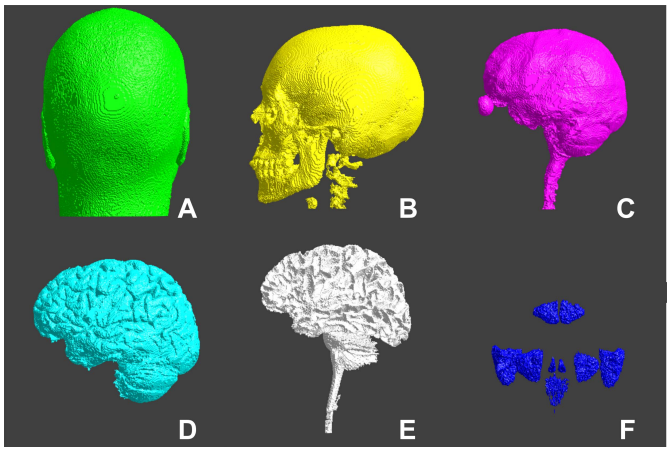

Fig. 8. The resulting 3D tissue models for subject no. 8: skin (A), skull (B), cerebrospinal fluid (C), grey matter (D), white matter (E), air-filled cavities (F).

and air-filled cavities. Detail of grey matter including ROI for all subject is shawn in Supplementary Figs. 2 and 3.

D. Results of Numerical Simulations

As stated in Sec. II-C.1, the success rate in rTMS patients suffering from orofacial pain is based on the ROI volume percentage where the induced electric field intensity exceeded 80 V/m, Fig. 9. To gain more information about the rTMS performed, we calculated the volume of the ROI before and after optimization where electric field intensity ranged from 0 to 170 V/m in 10 V/m intervals, see Supplementary Table III and IV. Table II shows the ROI volume for all 10 subjects with original and optimized coil targeting. Fig. 10 shows the calculated electric field intensity distribution induced in the grey matter model of subject no. 8. Electric field intensity distribution induced in the grey matter for all 10 subject is shown in Supplementary Fig. 1.

Table II lists for all 10 subjects the amplitude of the electric current flowing through the stimulation coil (I_C), the position of the coil center relative to the optimal position (Δx), the distance between the surface of the head and the edge of the region where an electric field with an intensity of 80 V/m was induced (D_{80}), the ROI volumes (V_{ROI}), and the total ROI volume before (ΣE_{ROI}) and after optimization (ΣE_{OPT}) as well as the the grey matter volume (ΣE_{GM}) stimulated by an

TABLE II
SIMULATION PARAMETERS THAT DESCRIBE THE RTMS TREATMENT COVERAGE OF THE ROI AND SURROUNDING GREY MATTER TISSUE

Subject No.	I_C(A)	Δx (mm)	D_{80} (mm)	V_{ROI} (cm^3)	ΣE_{ROI}(cm^3)	$\Sigma_{OPT(cm^3)}$	ΣE_{GM} (cm^3)
1	2574	26.9	23	1.089	0.000	0.651	24.803
2	2379	33.1	19	1.096	0.042	0.512	12.003
3	3042	15.5	34	0.914	0.111	0.398	26.677
4	3237	18.0	28	0.522	0.110	0.309	69.644
5	2379	10.9	28	0.392	0.021	0.129	14.435
6	2808	23.8	29	1.056	0.030	0.320	27.221
7	2184	5.0	10	1.306	0.000	0.551	4.877
8	2067	23.0	11	1.058	0.000	0.379	4.989
9	2964	33.5	24	0.673	0.000	0.273	35.688
10	1872	27.9	18	0.930	0.000	0.357	1.153
Average	2535	21.7	22	0.904	0.031	0.388	22.153

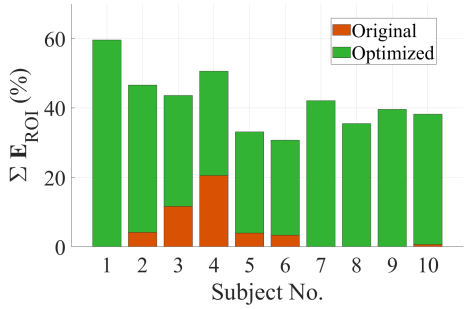

Fig. 9. Comparison of stimulating volume for original and optimized coil position. The original position corresponds to the one used in the rTMS treatment.

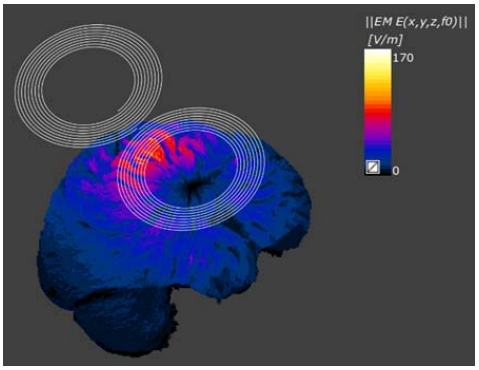

Fig. 10. Calculated electric field intensity distribution in the grey matter model of subject no. 8.

electric filed intensity over 80 V/m. ΣE_{ROI} (%) indicates the ratio of the stimulated ROI volume to the total ROI volume.

E. Analysis Results – Impact of Stimulation Coil Position on the Electric Field Induced in the ROI

Based on the results shown in Fig. 9, the analysis of impact of coil position to induced electric field in ROI was performed. As already described in Sec. II-C.2, the analysis was performed on subject no. 3 with an ROI volume closest to the mean. The results were evaluated using the same method as in Sec. III-D, shown in Figs. 11-13 and in more detail Supplementary Tables V - VIII.

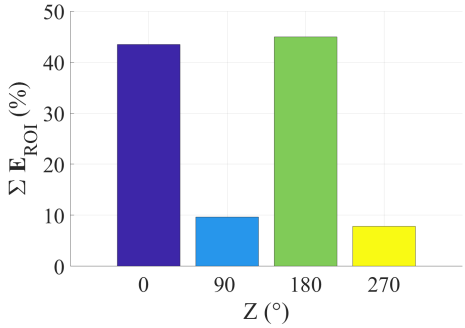

Fig. 11. Impact of rTMS stimulation coil rotation around the Z-axis on the induction of electric field intensity in ROI.

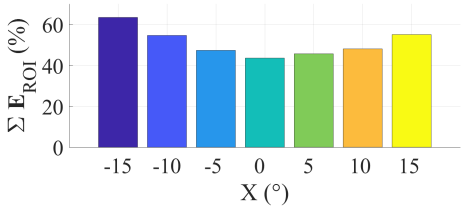

Fig. 12. Impact of rotating the rTMS coil around the X-axis on the E-field induced in the ROI.

The simulation results of coil rotation around the Z-axis are shown in Fig. 11. If the electric field vector was perpendicular to the gyrus, the induced electric field value increased. 43.6% and 45.0% of the ROI was stimulated at the initial stimulation coil angle and at 180°, respectively. On the other hand, at the stimulation coil angles of 90° and 270°, stimulation occurred only in 9.8% and 7.8% of the ROI, respectively.

Another analysed parameter was the rotation abround the X-axis from −15° to +15° with the results shown in Fig. 12 showing relatively symmetrical results, with the maximum ROI coverage at −15°. The results of the analysis of the impact of translation along the X- and Y-axes for the initial position on the electric field induced in the ROI are in Fig 13.

IV. DISCUSSION

A. Magnetic Field Generated by Stimulation Coil

The stimulation pulse wave form (Fig. 4) matched the wave form measured in [35], [36]. In all measured positions shown

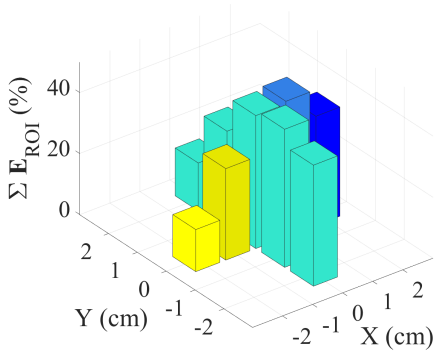

Fig. 13. Impact of translating the rTMS coil along the X- and Y-axis on the E-field induced in the ROI.

in Fig. 5, magnetic induction values were, on average, 28% lower. The stimulation intensity is adjusted by subject's motor threshold which is not affected by capacitor degradation. Such a marked difference between the measured and the simulated magnetic induction values can be likely attributed to capacitor degradation in the stimulation pulse generator, as the device has been in operation for over 10 years.

B. Magnetic Resonance and fMRI

Mechanical stimulation of patients during fMRI can activate motor response, which was observed in most patients. Other artifacts can be caused by the patient's movements, changes in oxygenation of individual structures due to thinking, feelings of fear, etc. These factors cannot be fully eliminated, it is therefore necessary to have the fMRI images processed by an interdisciplinary expert team. However, fMRI images of all patients showed activations in the sensory cortex where the ROI was anticipated. Diffusion tensor imaging and high performance computing would be needed to investigate the electric field in individual neurons.

C. 3D Scanning

According to the measurements performed, the 3D geometry acquired through scanning has proper dimensions and the relative error is lower than 2% of the respective dimension (Supplementary Table II). For a human head, this corresponds to an absolute error lower than 2 mm. There are local mesh integrity corruptions in the scanned model, but these have minimal impact on its overall usability. Main advantages of using the KINECT system includes the simplicity of operation, real-time scanning with the ability to review the model, accuracy, scanning speed and also the .STL output format which is supported by many CAD software tools.

D. Stimulation of Patients Suffering From Orofacial Pain

The rTMS application was assessed based on the calculated ROI volume, in which electric field intensity exceeded 80 V/m.

The examined ROI for all patients was a spatial body centred in the postcentral gyrus. According to current evidence [37], the sensory cortex located in postcentral gyrus is higly interconnected with many cortical and subcortical areas. Sensory cortex also has many more descending pathways than ascending ones so we can consider only minor effect of off-target stimulation to overall neural activity in ROI. For subject no. 1, however, the ROI was not exposed to electric field intensities above 80 V/m due to incorrect coil positioning. Subject no. 2 with a navigation error of 33.1 mm experienced stimulation in 4.1% of ROI volume. High values of electric field intensities are typically observed at the top of a gyrus. Based on the fMRI results, the ROI which represents the locus of orofacial pain isn't located only at the top of the gyrus. The subject no.2 reports initial pain fluctuation followed by subjective relief. The calculated navigation error for subject no. 3 was 15.5 mm and resulting in 11.6% ROI stimulation. With a depth of 33.1 mm, this subject achieved the deepest electric field with an intensity of 80 V/m. Subject no. 3 reported an occasional improvement by 2 points from 10-points scale after the procedure [5]. As for calculated values, subject no. 4's relatively low navigation error value of 18.0 mm, a small ROI with a volume of 522 mm^3 and highest stimulation current has resulted in the highest percentage of the stimulated ROI of 20.5%. Stimulation had a beneficial effect of improvement by 2 points on the scale. At the beginning, the pain limited the subject no. 4 in activities, now they performs activities without restrictions, even if they cannot be completely relieved from pain. The stimulation currents for subjects no. 5 and 6 induced electric fields of sufficient intensity, however the small ROI volume for subject no. 5 and the calculated navigation error for subject no. 6 prevented the stimulation from being a success. For subject no. 7, whose ROI was the largest, the smallest navigation error was achieved. According to calculated values, the stimulation was not successful due to low stimulation current which was unable to induce an electric field of sufficient intensity in sufficient depth. For subject no. 8, the stimulation depth was also not sufficient, again caused by low stimulation current. The highest navigation error was recorded for subject no. 9 (33.5 mm). Despite a high stimulation current and the fact that an electric field was able to stimulate the grey matter under the coil winding, the volume percent of stimulated ROI was equal to 0. For subject no. 10 the stimulated ROI volume was also negligible. Induction of an electric field of sufficient intensity in the ROI failed due to a relatively high navigation error coupled with a low stimulation current value. However, E-field coverage can be significantly improved via numerical simulations and optimization of the stimulation coil position as shown in Fig. 9. The resulting average value of the ROI volume stimulated by E-field intensity over 80 V/m increased from 4.3% (as used in the clinical scenario) to 43.0% (after retrospective optimization. Based on performed numerical calculations Magstim 70 mm Double Air Film Coil could stimulate up to 60% of patient's ROI. The volume of the total stimulated grey matter (ΣE_{GM}) is several times higher than the ROI volume (V_{ROI}), there could be an option to choose a stimulation current (I_C) around 2000 A, when the ratio of the stimulated ROI volume to the total volume grey matter volume is more favorable, as can be seen in Subjects 7, 8 and 10 (Supplementary Fig. 1).

E. Stimulation Coil Positioning Error

Although the Magstim 70 mm Double Air Film Coil stimulation coil was fixed to a holder and the patients were in a relaxed position, there was still a possiblilty of slight patient movement. Hypothetical treatment success rate could be increased by fixing both the stimualtion coil and the patient's head in place. For precise co-registration of the stimulation coil and an anatomically accurate head model it is always necessary to have a complete image matrix of the head including the ears, the nose and the crown. Neuronavigation systems bring the possibility of more precise stimulation coil positioning, on the other hand most of the available systems use only simplified models of the human brain. These systems can project individual anatomical MRI data on a scaled model despite the fact that the distribution of induced electric field does not include the individual brain anatomy. Therefore, individual numerical simulations of the induced electric field with anatomically accurate models will help achieve precise coil positioning for maximum stimulated ROI volume.

F. Impact of Stimulation Coil Position on Electric Field Induced in the ROI

The results of numerical simulations of the impact of coil rotation about the Z-axis (Fig.3B) confirmed that if the electric field vector is perpendicular to the gyrus, the induced electric field value increases (Fig. 11). After optimization, stimulated ROI volume percentage was 43.6% and 45.0% at 0° and at 180° Z-rotation, respectively. On the other hand, in the 90° and 270° position, the volume percentage of the stimulated ROI was negligible.

Rotating the stimulation coil around the X-axis (Fig. 3C) by ±5° and ±10° increases the volume of the stimulated ROI up to 47.4% and 54.7%, respectively (Fig. 12). Rotation by +15° increased the calculated values of electric field intensity up to 63.5%, which is almost 20% more comparing to initial position.

If the coil is moved along the positive Y-axis (see Supplementary Table VIII), in the direction of vertex, the volume in which stimulation provides electric filed with an intensity over 80 V/m decreases from 43.6% to 32.3% after 1 cm translation to 15.7% after 2 cm translation (Fig. 13). The negative direction of the Y-axis also follows the same gyrus where the ROI is located. When the coil is moved by 1 cm along the negative Y-axis, the stimulated ROI volume even slightly increases to 45.3%, and when moved by 2 cm, the stimulated volume decreases back to 39.7% which is almost the same value as in initial position. Motion in the positive direction along the X-axis (see Supplementary Table VII) moves the coil towards nasion and it does not affect the ROI stimulation coverage significantly: 44.5% and 35.8% for a 1 cm and 2 cm translation, respectively. When moving in the negative direction along the X-axis, the coil ends up outside the gyrus, translation by one centimeter decreases the stimulated volume to 30.0% and translation by two centimeters even leads to a reduction to 13.8%. If translation follows along the gyrus, the stimulated ROI volume percentage changes more smoothly with coil movement. If the coil is moved away from the gyrus with an error greater than two centimeters, the stimulation effect is almost entirely gone. Considering the average size of the ROI and the relatively high focality of the 70 mm Double Air Film stimulation coil, a possible solution might be using a circular coil that would stimulate a larger area of the grey matter. It would be necessary, however, to evaluate the impact of stimulation on the unintended parts of the brain.

We also performed the translation and rotation analysis for a 90° position, but the stimulated ROI volume was negligible and thus not reported.

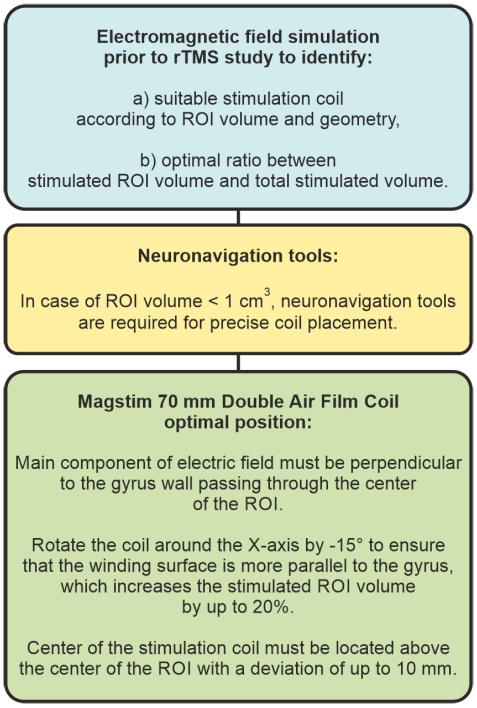

Fig. 14. Summary of the steps to maximize the accuracy of the rTMS application.

V. Conclusion

This research paper aimed to retrospectively simulate the electric field intensity in ROIs of 10 subjects undergoing rTMS for the possible treatment of orofacial pain and to evaluate the accuracy of the rTMS application. The delineation of the ROIs was successfully performed using fMRI images resulting in volumes ROI spanning from 673 to 1306 mm^3. The ROI were all located in the somatosensory cortex, which is activated during orofacial pain and that can be inhibited via rTMS. The combination of 3D scanning, MARS and iSeg segmentation as well as the Sim4Life numerical simulator enabled us to create an accurate numerical model and simulation results within six hours per patient. The simulations of electric field distribution in the patients' ROIs show that only 4.3% of the ROI volume was stimulated with an intensity of over 80 V/m.

After performing an optimization of the position and orientation of the coil relative to the patient head, the ROI coverage increased to 43.0% on average for all patients. Overall, our patient-specific numerical treatment planning approach

shows the ability to detect suboptimal coil positioning and thus increase treatment effectiveness. These two aspects will ultimately help improving clinical outcomes for patients with orofacial pain.

REFERENCES

[1] A. Aleman, "Use of repetitive transcranial magnetic stimulation for treatment in psychiatry," *Clin. Psychopharmacol. Neurosci.*, vol. 11, no. 2, pp. 53–59, 2013.

[2] J. Liepert, S. Zittel, and C. Weiller, "Improvement of dexterity by single session low-frequency repetitive transcranial magnetic stimulation over the contralesional motor cortex in acute stroke: A double-blind placebo-controlled crossover trial," *Restorative Neurol. Neurosci.*, vol. 25, nos. 5–6, pp. 461–465, 2007.

[3] M. Hallet, "Transcranial magnetic stimulation and the human brain," *Nature*, vol. 406, no. 6792, pp. 147–150, Jul. 2000.

[4] A. T. Barker, R. Jalinous, and I. L. Freeston, "Non-invasive magnetic stimulation of human motor cortex," *Lancet*, vol. 1, no. 8437, pp. 1106–1107, May 1985.

[5] J. Fricová, M. Klírová, V. Masopust, T. Novák, K. Vérebová, and R. Rokyta, "Repetitive transcranial magnetic stimulation in the treatment of chronic orofacial pain," *Physiolog. Res.*, vol. 62, pp. S125–S134, Nov. 2013.

[6] M. M. Klein *et al.*, "Transcranial magnetic stimulation of the brain: Guidelines for pain treatment research," *Pain*, vol. 156, no. 9, pp. 1601–1614, Sep. 2015.

[7] K. A. Follett and M. D. Mann, "Effective stimulation distance for current from macroelectrodes," *Experim. Neurol.*, vol. 92, no. 1, pp. 75–91, Apr. 1986. [Online]. Available: http://www.sciencedirect.com/science/article/pii/0014488686901263

[8] T. Kowalski, J. Silny, and H. Buchner, "Current density threshold for the stimulation of neurons in the motor cortex area," *Bioelectromagnetics*, vol. 23, no. 6, pp. 421–428, Sep. 2002, doi: 10.1002/bem.10036.

[9] B. J. Roth, L. G. Cohen, and M. Hallett, "The electric field induced during magnetic stimulation," *Electroencephalogr. Clin. Neurophysiol. Suppl.*, vol. 43, pp. 268–278, Jan. 1991.

[10] K.-H. Hsu, S. S. Nagarajan, and D. M. Durand, "Analysis of efficiency of magnetic stimulation," *IEEE Trans. Biomed. Eng.*, vol. 50, no. 11, pp. 1276–1285, Nov. 2003.

[11] J. Buday *et al.*, "Seizure threshold manipulation in electroconvulsive therapy via repetitive transcranial magnetic stimulation. A novel way of augmentation?" *Brain Stimulation*, vol. 13, no. 6, pp. 1631–1638, Nov. 2020. [Online]. Available: https://pubmed.ncbi.nlm.nih.gov/32977025/

[12] A. M. Janssen, T. F. Oostendorp, and D. F. Stegeman, "The coil orientation dependency of the electric field induced by TMS for M1 and other brain areas," *J. NeuroEng. Rehabil.*, vol. 12, no. 1, p. 47, May 2015.

[13] A. M. Janssen, T. F. Oostendorp, and D. F. Stegeman, "The effect of local anatomy on the electric field induced by TMS: Evaluation at 14 different target sites," *Med. Biol. Eng. Comput.*, vol. 52, no. 10, pp. 873–883, Oct. 2014.

[14] K. Porzig, H. Brauer, and H. Toepfer, "The electric field induced by transcranial magnetic stimulation: A comparison between analytic and FEM solutions," *Serbian J. Electr. Eng.*, vol. 11, no. 3, pp. 403–418, 2014.

[15] X. Zhong, P. Rastogi, Y. Wang, E. G. Lee, and D. Jiles, "Investigating the role of coil designs and anatomical variations in cerebellar TMS," *IEEE Trans. Magn.*, vol. 55, no. 7, pp. 1–5, Jul. 2019.

[16] A. Christ *et al.*, "The virtual family—Development of surface-based anatomical models of two adults and two children for dosimetric simulations," *Phys. Med. Biol.*, vol. 55, no. 2, pp. N23–N38, Jan. 2010.

[17] V. Guadagnin, M. Parazzini, S. Fiocchi, I. Liorni, and P. Ravazzani, "Deep transcranial magnetic stimulation: Modeling of different coil configurations," *IEEE Trans. Biomed. Eng.*, vol. 63, no. 7, pp. 1543–1550, Jul. 2016.

[18] M. Lu and S. Ueno, "Computational study toward deep transcranial magnetic stimulation using coaxial circular coils," *IEEE Trans. Biomed. Eng.*, vol. 62, no. 12, pp. 2911–2919, Dec. 2015.

[19] E. P. Bastings *et al.*, "Co-registration of cortical magnetic stimulation and functional magnetic resonance imaging," *NeuroReport*, vol. 9, no. 9, pp. 1941–1946, Jun. 1998.

[20] F. Fanjul-Vélez, I. Salas-García, N. Ortega-Quijano, and J. L. Arce-Diego, "FDTD-based transcranial magnetic stimulation model applied to specific neurodegenerative disorders," *Comput. Methods Programs Biomed.*, vol. 118, no. 1, pp. 34–43, Jan. 2015.

[21] R. Salvador, S. Silva, P. J. Basser, and P. C. Miranda, "Determining which mechanisms lead to activation in the motor cortex: A modeling study of transcranial magnetic stimulation using realistic stimulus waveforms and sulcal geometry," *Clin. Neurophysiol.*, vol. 122, no. 4, pp. 748–758, Apr. 2011.

[22] J. Vrba *et al.*, "Modeling of brain tissue heating caused by direct cortical stimulation for assessing the risk of thermal damage," *IEEE Trans. Neural Syst. Rehabil. Eng.*, vol. 27, no. 3, pp. 440–449, Mar. 2019.

[23] S. Mukesh, D. T. Blake, B. J. McKinnon, and P. T. Bhatti, "Modeling intracochlear magnetic stimulation: A finite-element analysis," *IEEE Trans. Neural Syst. Rehabil. Eng.*, vol. 25, no. 8, pp. 1353–1362, Aug. 2017.

[24] M. Cvetkovic, D. Poljak, and J. Haueisen, "Analysis of transcranial magnetic stimulation based on the surface integral equation formulation," *IEEE Trans. Biomed. Eng.*, vol. 62, no. 6, pp. 1535–1545, Jun. 2015.

[25] Microsoft. (2016). *Kinect Fusion Manual*. [Online]. Available: https://msdn.microsoft.com/en-us/library/dn188670.aspx/

[26] M. Ulvr, "Design of PCB search coils for AC magnetic flux density measurement," *AIP Adv.*, vol. 8, no. 4, Apr. 2018, Art. no. 047505, doi: 10.1063/1.4991643.

[27] Y. Huang and L. C. Parra, "Fully automated whole-head segmentation with improved smoothness and continuity, with theory reviewed," *PLoS ONE*, vol. 10, no. 5, May 2015, Art. no. e0125477.

[28] The FIL Methods Group. (2018). *SPM Statistical Parametric Mapping Manual*. [Online]. Available: http://www.fil.ion.ucl.ac.U.K./spm/

[29] *iSEG User's Manual*, Zurich MedTech AG, Zürich, Switzerland, 2020.

[30] C. Gabriel, "Compilation of the dielectric properties of body tissues at RF and microwave frequencies," King's College, London, U.K., 1996, doi: 10.21236/ada303903.

[31] P. A. Hasgall *et al.* (2018). *Tissue Properties Database V4.0*. [Online]. Available: www.itis.ethz.ch/database

[32] *Sim4life User's Manual*, Zurich MedTech AG, Zürich, Switzerland, 2020.

[33] Magstim. (2019). *Magstim Rapid2*. [Online]. Available: www.magstim.com/product/rapid-family/

[34] T. Radman, R. L. Ramos, J. C. Brumberg, and M. Bikson, "Role of cortical cell type and morphology in subthreshold and suprathreshold uniform electric field stimulation *in vitro*," *Brain Stimulation*, vol. 2, no. 4, pp. 215–228, Oct. 2009.

[35] T. Kammer, S. Beck, A. Thielscher, U. Laubis-Herrmann, and H. Topka, "Motor thresholds in humans: A transcranial magnetic stimulation study comparing different pulse waveforms, current directions and stimulator types," *Clin. Neurophysiol.*, vol. 112, no. 2, pp. 250–258, 2001. [Online]. Available: https://linkinghub.elsevier.com/retrieve/pii/S1388245700005137

[36] A. V. Peterchev *et al.*, "Fundamentals of transcranial electric and magnetic stimulation dose: Definition, selection, and reporting practices," *Brain Stimulation*, vol. 5, no. 4, pp. 435–453, Oct. 2012. [Online]. Available: https://www.ncbi.nlm.nih.gov/pmc/articles/PMC3346863/

[37] E. Kropf, S. K. Syan, L. Minuzzi, and B. N. Frey, "From anatomy to function: The role of the somatosensory cortex in emotional regulation," *Brazilian J. Psychiatry*, vol. 41, no. 3, pp. 261–269, May 2019.